Two-Loop Electroweak Corrections with Fermion Loops to $e^+e^- \to ZH$

Ayres Freitas[*] and Qian Song[†]

Pittsburgh Particle-physics Astro-physics and Cosmology Center (PITT-PACC) Department of Physics and Astronomy, University of Pittsburgh, Pittsburgh, Pennsylvania 15260, USA

We present a complete calculation of the next-to-next-to-leading electroweak corrections involving closed fermion loops to $e^+e^- \to ZH$. This has been achieved by using a seminumerical technique for the two-loop vertex and box diagrams, based on Feynman parameters and dispersion relations for one of the two subloops. UV divergences are treated with suitable subtraction terms. Numerical results for the unpolarized differential and integrated cross section at center-of-mass energy 240 GeV are provided. The new corrections are found to increase the predicted cross section by 0.7%.

Introduction.—After the discovery of the Higgs boson [1,2] at the Large Hadron Collider (LHC) in 2012, it will be crucial to perform precision studies of its properties, in order to understand the details of the mechanism of electroweak symmetry breaking and search for signs of new physics beyond the Standard Model (SM). Possible deviations of Higgs couplings from the SM expectations may appear at the percent level in a wide range of models [3].

For this purpose, several proposals have been made for so-called e^+e^- Higgs factories: the International Linear Collider (ILC) [4,5], the Future Circular Collider (FCC-ee) [6], and the Circular Electron-Positron Collider (CEPC) [7]. Those colliders are intended to operate at center-of-mass energies of 240–250 GeV, in which the Higgsstrahlung process, $e^+e^- \to ZH$, becomes the dominant Higgs production channel. As a result of a clean environment and high luminosity, the cross section for ZH production is expected to be measured with a precision of about 1.2% at ILC, 0.4% at FCC-ee, and 0.5% at CEPC.

To extract the coupling between Higgs and Z boson, theoretical predictions for the process $(e^+e^- \to ZH)$ are necessary, and the precision should be at least of the same order as the experimental one. Within the SM, leading order (LO) [8] and next-to-leading order (NLO) corrections have been known for a long time for unpolarized beams [9–11], and more recently for polarized beams [12]. The effects of multiple collinear photon emission in the initial state, which are enhanced by powers of $\log(s/m_e^2)$, can be taken into account with Monte-Carlo [13] or structure function [14] methods. Other higher-order corrections are more challenging to compute. The mixed electroweak-QCD [$\mathcal{O}(\alpha\alpha_s)$] correction has been calculated by two groups independently [15,16]. Furthermore, the NLO and next-to-next-to-leading order(NNLO) $\mathcal{O}(\alpha\alpha_s)$ corrections have also been computed for the final state of $\mu\bar{\mu}H$, i.e., including Z decays into dimuon pairs [17]. The $\mathcal{O}(\alpha\alpha_s)$ correction was found to be about 1.5% of the LO result, which is significantly larger than the expected experimental accuracy of CEPC and FCC-ee.

The most important missing higher-order corrections are NNLO electroweak corrections, which are expected to contribute at the percent level and thus comparable or larger than the experimental precision of future Higgs factories. This Letter presents the complete calculation of NNLO corrections based on two-loop electroweak diagrams with closed fermion loops. Closed fermion loops contributions are typically dominant because of the large top-quark Yukawa coupling and the large number of fermion flavors in the SM, which is corroborated by previous calculations [18,19]. With difficulties in finding analytical solutions, numerical methods allow broader flexibility. Recent innovative techniques based on series solutions of differential equations [20–23] seems promising, but they rely on integration-by-parts reduction, which is typically the computational bottleneck.

Our calculation is based on a seminumerical method using a combination of dispersion relations and Feynman parametrizations, which was first introduced in Ref. [24] for the evaluation of two-loop double boxes. The method has been further developed to enable the treatment of UV divergences, which occur in two-loop vertex integrals and subloop vertex and self-energy contributions. Integration-by-parts reduction is not needed. With our approach all relevant two-loop diagrams are reduced to at most three-dimensional numerical integrals that can be evaluated with typically three-to-four digit precision within minutes on a
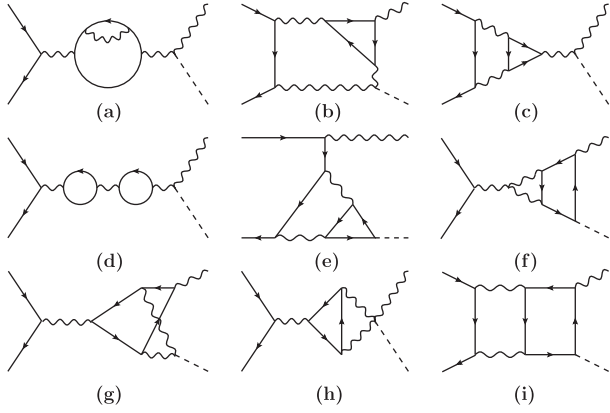
FIG. 1. Examples of two-loop Feynman diagrams with at least one closed fermion loop.

single CPU core [or up to a few hours when using quadruple-precision numbers for higher accuracy]. To the best of our knowledge, this is the first computation of NNLO electroweak corrections to a $2 \to 2$ scattering cross section.

Method.—Two-loop electroweak diagrams with fermion loops can be classified into vertex, self-energy, box, and reducible two-loop diagrams. Some example diagrams are shown in Fig. 1. Many of these diagrams are infrared (IR) and/or ultraviolet (UV) divergent. IR divergences can be spurious or physical. The former cancel in a subset of similar diagrams, but they must be regulated in individual diagrams, which we achieve by introducing a small fictitious photon mass. The physical IR divergences only emerge from initial-state QED vertex corrections, and they cancel against real photon emission contributions. However, initial-state QED corrections factorize and can be taken into account through convolution with process-independent structure functions; see, e.g., Ref. [14]. Therefore we omit these contribution in our calculation. Dimensional regularization is employed to regulate the UV divergence. It is worthwhile to briefly discuss the renormalization scheme and the treatment of γ_5 in D dimensions.

We employed on-shell renormalization scheme for all fields, masses, and electromagnetic coupling e. The $\alpha(0)$ scheme is used for the latter, i.e., e is normalized to its value in the Thomson limit. As a result, the final result depends on the shift $\Delta\alpha = 1 - \alpha(m_Z)/\alpha(0)$, where $\alpha(\mu)$ is the running electromagnetic coupling at the sale μ. More details on the renormalization parameters can be found in Ref. [25].

The problem of γ_5 appears in the diagrams involving triangle fermion loops, which require the evaluation of $\mathrm{tr}(\gamma^\alpha\gamma^\beta\gamma^\mu\gamma^\nu\gamma_5)$. In D dimensions, the anticommutation relation $\{\gamma^\mu, \gamma_5\}$ and the trace identity $\mathrm{tr}(\gamma^\alpha\gamma^\beta\gamma^\mu\gamma^\nu\gamma_5) = -4i\epsilon^{\alpha\beta\mu\nu}$ cannot be satisfied simultaneously. However, contributions originating from the ϵ tensor are UV finite, so they can be safely evaluated in four dimensions.

This approach has been used for example in Refs. [18,26]. More strategies about the treatment of γ_5 in D dimensions can be found in Ref. [27].

Now let us discuss the evaluation of the two-loop integrals in the matrix element for $e^+e^- \to ZH$. The reducible diagrams, Fig. 1(d), and self-energy diagrams, Fig. 1(a), can be straightforwardly computed by reducing the expressions to a set of known master integrals (MIs) [28]. The MIs have been evaluated numerically using LOOPTOOLS 2.16 [29] for the one-loop cases and TVID 2.2 [30] for the two-loop self-energies. The two-loop counterterms have been computed with the same approach.

For the two-loop vertex and box diagrams, we adopt the method of Ref. [24], which has been extended to deal with UV-divergent diagrams. The approach uses Feynman parameters to transform one of the two subloops into a self-energy-type integral, which can be expressed in terms of a dispersion relation. The second subloop can then be solved analytically via well-known one-loop Passarino-Veltman functions. No reduction to MIs is required in this approach. The integration over the Feynman and dispersion parameters is performed numerically, resulting in at most three-dimensional integrals for two-loop vertex and box diagrams.

UV divergences need to be subtracted before carrying out the numerical integration. In general, three types of subtraction terms may be needed, two for subloop divergences and one more for a global (or nested) divergence. [The number of subtraction terms varies with topologies; for simpler topologies, only one term is needed.] The subtraction terms should be simple enough to be integrated analytically and then added back to the total result.

To illustrate how to subtract the UV divergences, let us take an example from the diagram shown in Fig. 1(f), namely the tensor function given in Eq. (1) below. By power counting one can see that this integral has subloop divergences for both the q_1 and q_2 loops, as well as a global two-loop divergence. After introducing a Feynman parameter and shifting the q_2 momentum, one arrives at the expression in Eq. (2), where $p_x = xp = x(p_z + p_h)$ and $m_x^2 = (1-x)m_{V_2}^2 + xm_{V_1}^2 + (x^2 - x)p^2$. Here p_z and p_h are the momenta of the final-state Z boson and Higgs boson, respectively, whereas p is the s-channel momentum. Next, the q_2 loop is rewritten in terms of dispersion relations. This produces a number of terms, of which only the divergent ones are explicitly shown in Eq. (3). The remaining terms, denoted by $\mathcal{I}_{q_1,q_2}^{\mathrm{finite}}$, are finite and do not play any role in the UV subtraction. Here $\sigma_0 = (m_x + m_{f_1})^2$, and the explicit form of the dispersion kernels ΔB_{ij} can be found in Ref. [24]. For future reference, we introduce the symbols $\mathcal{I}_{q_1}^{ij}$ for the three q_1 integrals in Eq. (3).

$$\mathcal{I} = \int \frac{d^D q_2}{i\pi^2} \frac{d^D q_1}{i\pi^2} \frac{q_2^2 q_1^2 + q_1^4}{(q_2^2 - m_{V_2}^2)[(q_2 + p)^2 - m_{V_1}^2][(q_2 + q_1)^2 - m_{f_1}^2](q_1^2 - m_{f_2}^2)[(q_1 - p_h)^2 - m_{f_2}^2][(q_1 - p)^2 - m_{f_2}^2]} \quad (1)$$

$$= \int_0^1 dx \int \frac{d^D q_2}{i\pi^2} \frac{d^D q_1}{i\pi^2} \frac{(q_2 - p_x)^2 q_1^2 + q_1^4}{(q_2^2 - m_x^2)^2[(q_2 + q_1 - p_x)^2 - m_{f_1}^2](q_1^2 - m_{f_2}^2)[(q_1 - p_h)^2 - m_{f_2}^2][(q_1 - p)^2 - m_{f_2}^2]} \quad (2)$$

$$= \int_0^1 dx \int \frac{d^D q_1}{i\pi^2} \int_{\sigma_0}^{\infty} d\sigma \frac{\partial}{\partial m_x^2} \left(\frac{q_1^4 \Delta B_0(\sigma, m_x^2, m_{f_1}^2) + q_1^2 \Delta B_{00}(\sigma, m_x^2, m_{f_1}^2) + q_1^4 \Delta B_{11}(\sigma, m_x^2, m_{f_1}^2)}{(q_1^2 - m_{f_2}^2)[(q_1 - p_h)^2 - m_{f_2}^2][(q_1 - p)^2 - m_{f_2}^2][\sigma - (q_1 - p_x)^2]} \right) + \mathcal{I}_{q_1, q_2}^{\text{finite}} \quad (3)$$

The dispersion relation in Eq. (3) is valid only for $m_x^2 > 0$. When $m_x^2 < 0$, the dispersion relation is modified according to

$$\int_{\sigma_0}^{\infty} d\sigma \frac{\partial}{\partial m_x^2} \left(\frac{\Delta B_0(\sigma, m_x^2, m_{f_1}^2)}{[\sigma - (q_1 - p_x)^2]} \times \dots \right) \rightarrow \frac{1}{2\pi i} \int_{-\infty}^{\infty} d\sigma \frac{\partial}{\partial m_x^2} \left(\frac{B_0(\sigma, m_x^2, m_{f_1}^2)}{[\sigma - (q_1 - p_x)^2 - i\epsilon]} \times \dots \right), \text{etc.}, \quad (4)$$

where $i\epsilon$ is a small numerical value. It must be added because it ensures all Passarino-Veltman functions are properly define for all values of σ. We have confirmed that the result is independent of ϵ as long as it is small enough. More details about dispersion relation can be found in Ref. [24].

As mentioned above, $\mathcal{I}$ has a global divergence (when $q_{1,2} \to \infty$) and subloop divergences when either $q_1 \to \infty$ or $q_2 \to \infty$. The UV divergence from the q_1 loop is obtained by setting all other momenta inside q_1 propagators to zero. For instance, for the q_1^4 term in Eq. (2) this leads to

$$\mathcal{I}_{q_1}^{\text{div}} = \int \frac{d^D q_2}{i\pi^2} \frac{d^D q_1}{i\pi^2} \frac{1}{(q_2^2 - m_{V_2}^2)[(q_2 - p)^2 - m_{V_1}^2]}$$
$$\times \frac{q_1^4}{(q_1^2 - m_{f_2}^2)(q_1^2 - m_{f_2}^2)(q_1^2 - m_{f_2}^2)(q_1^2 - m_{f_1}^2)} \quad (5)$$

$$= B_0(p^2, m_{V_2}^2, m_{V_1}^2) \times [c_1 A_0(m_{f_1}^2) + c_2 A_0(m_{f_2}^2)], \quad (6)$$

where A_0 and B_0 are the usual one-loop MIs, and the c_i are functions of m_{f_1}, m_{f_2}, and the dimension D. The q_2 integral in Eq. (5) can be turned into a dispersion relation and combined with Eq. (3) to render the q_1 integration finite.

The q_2 subloop divergence is manifested as a divergence of the σ integral at its upper limit ($\sigma \to \infty$). In our example, the term $\partial_{m_x^2} \Delta B_{00}(\sigma, m_x^2, m_{f_1}^2)/[\sigma - (q_1 - p_x)^2]$ diverges when σ tends to infinity. However, $\partial_{m_x^2} \Delta B_{00}(\sigma, m_x^2, m_{f_1}^2) \times (\{1/[\sigma - (q_1 - p_x)^2]\} - [1/(\sigma - m^2)])$ is UV finite, where m^2 can be any arbitrary value (the simplest choice is $m^2 = 0$). So the divergence is eliminated by subtracting the following term:

$$\mathcal{I}_{q_2}^{\text{div}} = \int_0^1 dx \int \frac{d^D q_1}{i\pi^2} \int_{\sigma_0}^{\infty} d\sigma \frac{\partial}{\partial m_x^2} \frac{\Delta B_{00}(\sigma, m_x^2, m_{f_1}^2)}{\sigma - m^2} \frac{q_1^2}{\{(q_1^2 - m_{f_2}^2)[(q_1 - p_h)^2 - m_{f_2}^2][(q_1 - p)^2 - m_{f_2}^2]\}}$$
$$= \int_0^1 dx \frac{\partial}{\partial m_x^2} B_{00}(m^2, m_x^2, m_f^2) \times \int \frac{d^D q_1}{i\pi^2} \frac{q_1^2}{[\dots]}. \quad (7)$$

Both factors in the last line are one-loop functions that can be computed analytically, and only the x integration needs to be carried out numerically.

After subtraction of the two subloop divergences, one still needs to take care of the global UV divergence, which is canceled by subtracting the same integral with all external momenta set to zero ($p_z = p_h = 0$, $\therefore p_x = 0$). This produces vacuum integrals, which can easily be reduced to MIs, for which analytical formulas are known [31].

As we can see in Eq. (3), a derivative with respect to the mass square m_x^2 appears in the dispersion relations for two-loop vertex diagrams. Sometimes, for the global UV subtraction terms of diagrams with massless fermions, one can have $m_x^2 = 0$, which produces a singularity in the integrand. In such cases, a fictitious mass M needs to be introduced for the q_2, e.g.,

$$\mathcal{I}_{q_1 q_2}^{\text{div}} = \int \frac{d^D q_2}{i\pi^2} \frac{d^D q_1}{i\pi^2} \frac{1}{(q_2^2 - M^2)^2[(q_2 + q_1)^2 - m_{X_1}^2]}$$
$$\times \frac{q_1^4}{(q_1^2 - m_{X_2}^2)^3} \quad (8)$$

$$= \int \frac{d^D q_1}{i\pi^2} \frac{\partial B_0(q_1^2, M^2, m_{X_1}^2)}{\partial M^2} \frac{q_1^4}{(q_1^2 - m_{X_2}^2)^3}. \quad (9)$$
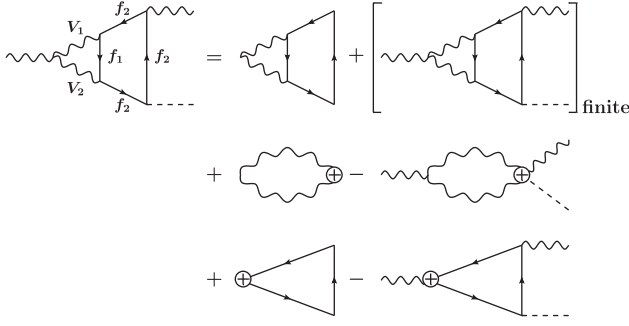
FIG. 2. Diagrammatical demonstration of VZH divergence separation. $[]_{\text{finite}}$ denotes the finite integral after all subtractions have been applied.

After adding the global subtraction term back analytically, the result does not depend on the value of M, which hence can be chosen arbitrarily. The UV subtraction process is diagrammatically demonstrated in Fig. 2. Diagrams without external lines correspond to vacuum diagrams. The diagrams in the second and third line are used to eliminate divergences in the subloop, which is symbolized as $\oplus$. They are the product of one-loop functions as shown in Eqs. (6) and (7).

The entire sequence of steps outlined above has been implemented in two independent ways to enable cross-checks. Feynman diagrams and amplitudes are generated in Feynman gauge with FEYNARTS [32] in both implementations. For the Lorentz and Dirac algebra, FEYNCALC [33] is employed in one implementation, and the results were cross-checked against a private code. The Feynman parametrization, construction of dispersion relations, and UV subtraction have been carried out in two independent private codes in MATHEMATICA. The UV-finite integrals are evaluated numerically in C++ with the help of LOOPTOOLS [29] and adaptive Gauss quadrature integration, again in two separate codes, one using the integration routine from the BOOST library [34], and the other utilizing the QUADPACK library [35]. For some cases with large numerical cancellations in the integrand, the integration was rerun using quadruple-precision numbers. As an additional cross-check, vertex diagrams with self-energy subloops and vertex diagrams with four-point vertices [see Fig. 1(h)] were also computed by reducing them to MIs and evaluating the latter with TVID [30].

Since the Z boson width Γ_Z is relatively large, it cannot be treated as an asymptotic on-shell state. Instead, the results for the production cross section presented here correspond to the leading term in an expansion about the complex pole $s_0 = m_Z^2 - im_Z\Gamma_Z$. More details can be found in the Supplemental Material [36].

It is worth noting that the complex pole expansion leads to a definition for the Z mass and width that differs from the one that is commonly used in experimental studies. The relation between the two is given by [41]

$$m_Z = m_Z^{\text{exp}}[1 + (\Gamma_Z^{\text{exp}}/m_Z^{\text{exp}})^2]^{-1/2}, \quad (10)$$

$$\Gamma_Z = \Gamma_Z^{\text{exp}}[1 + (\Gamma_Z^{\text{exp}}/m_Z^{\text{exp}})^2]^{-1/2}. \quad (11)$$

Results.—The following input parameters are used for the numerical evaluation:

$$
\begin{aligned}
m_W^{\text{exp}} &= 80.379 \,\text{GeV} \;\Rightarrow\; m_W = 80.352 \,\text{GeV}, \\
m_Z^{\text{exp}} &= 91.1876 \,\text{GeV} \;\Rightarrow\; m_Z = 91.1535 \,\text{GeV}, \\
m_H &= 125.1 \,\text{GeV}, \quad m_t = 172.76 \,\text{GeV}, \\
\alpha^{-1} &= 137.036, \quad \Delta\alpha = 0.059, \quad \sqrt{s} = 240 \,\text{GeV}. \quad (12)
\end{aligned}
$$

where $\sqrt{s}$ represents the center-of-mass energy, and the masses of all the other fermions are set to be 0.

Table I lists the results for the integrated unpolarized cross section at LO, NLO, and NNLO, where corrections are further divided according to the number of closed fermion loops, denoted by N_f. One can see that corrections with more fermion loops dominate. At the NLO, contributions from fermionic and bosonic corrections partially cancel, resulting in an increase of σ_{LO} by 3%. The NNLO electroweak corrections turn out to be 0.7% of the NLO correction, where the contribution with two fermion loops is much greater than the one with one fermion loop. This can be partially explained as a consequence of large top mass and flavor number enhancement of each fermion loop. In addition, there is an accidental numerical cancellation in the differential cross section for the $N_f = 1$ contribution. This can be clearly seen in Fig. 3, where we plot the unpolarized differential cross section at LO, NLO, and NNLO as a function of the scattering angle. The contribution due to $N_f = 1$ (i.e., the difference between the solid blue and dash-dotted green curves) is positive in the central region, $0.3\pi < \theta < 0.7\pi$, and negative in the forward and backward regions, where it can reach almost -3% of the LO result.

As a consequence of this, the shape of the angular dependence in Fig. 3 is changed slightly at NNLO in

TABLE I. Numerical results for the integrated cross section at LO, NLO, and NNLO. Electroweak one-loop and two-loop corrections are also provided and divided according to the number of fermion loops symbolized as N_f.

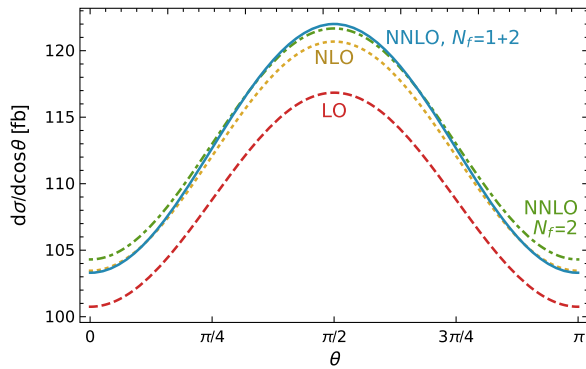|	(fb)	Contribution	(fb)
σ^{LO}	222.958		
σ^{NLO}	229.893		
		$\mathcal{O}(\alpha_{N_f=1})$	21.130
		$\mathcal{O}(\alpha_{N_f=0})$	−14.195
σ^{NNLO}	231.546		
		$\mathcal{O}(\alpha_{N_f=2}^2)$	1.881
		$\mathcal{O}(\alpha_{N_f=1}^2)$	−0.226

FIG. 3. Differential unpolarized cross section at $\sqrt{s} = 240$ GeV at LO, NLO and NNLO.

comparison to LO and NLO. This distortion mainly originates from the final-state $ZZH/\gamma ZH$ vertex and box diagrams.

Conclusions.—Motivated by the anticipated high precision for the measurement of $\sigma(e^-e^+ \to ZH)$, in this Letter we present the complete calculation of NNLO electroweak corrections with closed fermion loops. We found that they change the NLO results by 0.7% in the $\alpha(0)$ scheme, which is comparable with the expected precision of future Higgs factories. The NNLO results can be further divided according to the number of fermion loops, and the contribution with two closed fermion loops dominates over the one with one closed fermion loop. The calculation was made possible by a new seminumerical technique for the evaluation of two-loop box and vertex diagrams. Although the efficacy of our method has only been demonstrated by evaluating diagrams with fermion loops, the bosonic corrections require no new technical concept and thus can also be computed with our method. Besides, our method could also be applied to NNLO electroweak corrections for other scattering processes.

---

[*]afreitas@pitt.edu
[†]qis26@pitt.edu

[1] G. Aad *et al.* (ATLAS Collaboration), Observation of a new particle in the search for the Standard Model Higgs boson with the ATLAS detector at the LHC, Phys. Lett. B **716**, 1 (2012).
[2] S. Chatrchyan *et al.* (CMS Collaboration), Observation of a new boson at a mass of 125 GeV with the CMS experiment at the LHC, Phys. Lett. B **716**, 30 (2012).
[3] C. Englert, A. Freitas, M. M. Mühlleitner, T. Plehn, M. Rauch, M. Spira, and K. Walz, Precision measurements of Higgs couplings: Implications for new physics scales, J. Phys. G **41**, 113001 (2014).
[4] H. Baer *et al.*, The international linear collider technical design report—volume 2: Physics, arXiv:1306.6352.
[5] P. Bambade *et al.*, The international linear collider: A global project, arXiv:1903.01629.
[6] A. Abada *et al.* (FCC Collaboration), FCC-ee: The lepton collider: Future circular collider conceptual design report volume 2, Eur. Phys. J. Special Topics **228**, 261 (2019).
[7] J. B. Guimarães da Costa *et al.* (CEPC Study Group), CEPC conceptual design report: Volume 2—physics & detector, arXiv:1811.10545.
[8] B. W. Lee, C. Quigg, and H. B. Thacker, Weak interactions at very high energies: The role of the Higgs-boson mass, Phys. Rev. D **16**, 1519 (1977).
[9] J. Fleischer and F. Jegerlehner, Radiative corrections to Higgs production by $e^+e^- \to ZH$ in the Weinberg-Salam model, Nucl. Phys. **B216**, 469 (1983).
[10] B. A. Kniehl, Radiative corrections for associated ZH production at future e^+e^- colliders, Z. Phys. C **55**, 605 (1992).
[11] A. Denner, J. Küblbeck, R. Mertig, and M. Böhm, Electroweak radiative corrections to $e^+e^- \to ZH$, Z. Phys. C **56**, 261 (1992).
[12] S. Bondarenko, Y. Dydyshka, L. Kalinovskaya, L. Rumyantsev, R. Sadykov, and V. Yermolchyk, One-loop electroweak radiative corrections to polarized $e^+e^- \to ZH$, Phys. Rev. D **100**, 073002 (2019).
[13] C. Chen, Z. Cui, G. Li, Q. Li, M. Ruan, L. Wang, and Q. s. Yan, $H \to e^+e^-$ at CEPC: ISR effect with MadGraph, arXiv:1705.04486.
[14] M. Greco, G. Montagna, O. Nicrosini, F. Piccinini, and G. Volpi, ISR corrections to associated HZ production at future Higgs factories, Phys. Lett. B **777**, 294 (2018).
[15] Y. Gong, Z. Li, X. Xu, L. L. Yang, and X. Zhao, Mixed QCD-EW corrections for Higgs boson production at e^+e^- colliders, Phys. Rev. D **95**, 093003 (2017).
[16] Q. F. Sun, F. Feng, Y. Jia, and W. L. Sang, Mixed electroweak-QCD corrections to e + e− → HZ at Higgs factories, Phys. Rev. D **96**, 051301(R) (2017).
[17] W. Chen, F. Feng, Y. Jia, and W. L. Sang, Mixed electroweak-QCD corrections to $e^+e^- \to \mu^+\mu^-H$ at CEPC with finite-width effect, Chin. Phys. C **43**, 013108 (2019).
[18] M. Awramik, M. Czakon, and A. Freitas, Electroweak two-loop corrections to the effective weak mixing angle, J. High Energy Phys. 11 (2006) 048.
[19] I. Dubovyk, A. Freitas, J. Gluza, T. Riemann, and J. Usovitsch, Complete electroweak two-loop corrections to Z boson production and decay, Phys. Lett. B **783**, 86 (2018).
[20] F. Moriello, Generalised power series expansions for the elliptic planar families of Higgs + jet production at two loops, J. High Energy Phys. 01 (2020) 150.
[21] M. Hidding, DiffExp, a Mathematica package for computing Feynman integrals in terms of one-dimensional series expansions, Comput. Phys. Commun. **269**, 108125 (2021).
[22] X. Liu and Y. Q. Ma, AMFlow: A Mathematica package for Feynman integrals computation via auxiliary mass flow, Comput. Phys. Commun. **283**, 108565 (2023).

[23] T. Armadillo, R. Bonciani, S. Devoto, N. Rana, and A. Vicini, Evaluation of Feynman integrals with arbitrary complex masses via series expansions, Comput. Phys. Commun. **282,** 108545 (2023).

[24] Q. Song and A. Freitas, On the evaluation of two-loop electroweak box diagrams for $e^+e^- \to HZ$ production, J. High Energy Phys. 04 (2021) 179.

[25] A. Freitas, W. Hollik, W. Walter, and G. Weiglein, Electroweak two loop corrections to the $M_W - M_Z$ mass correlation in the standard model, Nucl. Phys. **B632,** 189 (2002).

[26] Y. Du, A. Freitas, H. H. Patel, and M. J. Ramsey-Musolf, Parity-Violating Møller Scattering at Next-to-Next-to-Leading Order: Closed Fermion Loops, Phys. Rev. Lett. **126,** 131801 (2021).

[27] F. Jegerlehner, Facts of life with gamma(5), Eur. Phys. J. C **18,** 673 (2001).

[28] G. Weiglein, R. Scharf, and M. Bohm, Reduction of general two loop selfenergies to standard scalar integrals, Nucl. Phys. **B416,** 606 (1994).

[29] T. Hahn and M. Perez-Victoria, Automatized one loop calculations in four-dimensions and D-dimensions, Comput. Phys. Commun. **118,** 153 (1999).

[30] S. Bauberger, A. Freitas, and D. Wiegand, TVID 2: Evaluation of planar-type three-loop self-energy integrals with arbitrary masses, J. High Energy Phys. 01 (2020) 024.

[31] A. I. Davydychev and J. B. Tausk, Two loop selfenergy diagrams with different masses and the momentum expansion, Nucl. Phys. **B397,** 123 (1993).

[32] T. Hahn, Generating Feynman diagrams and amplitudes with FeynArts 3, Comput. Phys. Commun. **140,** 418 (2001).

[33] V. Shtabovenko, R. Mertig, and F. Orellana, New developments in FeynCalc 9.0, Comput. Phys. Commun. **207,** 432 (2016).

[34] N. Agrawal *et al.*, Boost Math Toolkit 2.13.0, www.boost.org/doc/libs/master/libs/math/doc/html/index.html.

[35] R. Piessens, E. de Doncker-Kapenga, C. W. Überhuber, and D. K. Kahanger, *QUADPACK, A Subroutine Package for Automatic Integration* (Springer, Berlin, 1983).

[36] See Supplemental Material at http://link.aps.org/supplemental/10.1103/PhysRevLett.130.031801 for a brief exposition of the complex-pole expansion, which includes Refs. [37–40].

[37] S. Willenbrock and G. Valencia, On the definition of the Z boson mass, Phys. Lett. B **259,** 373 (1991).

[38] A. Sirlin, Theoretical Considerations Concerning the Z0 Mass, Phys. Rev. Lett. **67,** 2127 (1991).

[39] R. G. Stuart, Gauge invariance, analyticity and physical observables at the Z0 resonance, Phys. Lett. B **262,** 113 (1991).

[40] H. G. J. Veltman, Mass and width of unstable gauge bosons, Z. Phys. C **62,** 35 (1994).

[41] D. Y. Bardin, A. Leike, T. Riemann, and M. Sachwitz, Energy dependent width effects in e+ e- annihilation near the Z boson pole, Phys. Lett. B **206,** 539 (1988).